Innovative methodology for the design of composite steel-concrete sections with a new proposal for EC3 part 2

L. Salvador[a*] and M.R.T. Arruda[b]

[a]Phd Student, Instituto Superior Técnico, Universidade de Lisboa, Portugal
[b]Research Associate, CERIS – Civil Engineering Research and Innovation for Sustainability, Instituto Superior Técnico, Universidade de Lisboa, Portugal

A R T I C L E I N F O	A B S T R A C T
	In this work, the study of the evolutive behaviour of composite steel-concrete sections used in bridge decks was performed. A new method is proposed for the annex of EC3 part 2, in order to study the evolution effective steel area in a composite section, for serviceability and ultimate states. A coherent theoretical framework is presented, based on several relevant codes, namely the new Eurocodes. With this framework, a computer program is developed taking into account several important aspects in the behaviour of steel-concrete composite sections, such as nonlinear stress-strain relationships of the materials, local buckling of steel plates, time-dependent effects in concrete behaviour and load history. Also a new algorithm is proposed in order to compute strain fields at the section level from a known set of internal forces in the section, in nonlinear constitutive relations. Results obtained with the developed computer program are presented for several examples of typical sections found in bridge decks. Those results include moment-curvature plots, evolution of the strain field, evolution of the neutral axis, evolution of the stress in some points of the section. The influence of the concrete ultimate resistance and the staged construction sequence in the behaviour of the section is also evaluated.

1. Introduction

In recent years the number of structures using composite sections, including bridges and viaducts, has increased considerably in Portugal (Reis, 1997, 1999). The main reasons are a better use of different materials and some interesting and competitive possibilities, regarding construction sequence (Pedro & Reis, 2010; Reis, 2005; Reis & Pedro, 2004). In urban viaducts where the downtime traffic pause is the main constrain (Anitori, Casas, & Ghosn, 2013; Bradford et al., 2001), the use of composite structures with prior metal assembly (Kim & Yoo, 2006), as proven to be an efficient solution, in which the steel part will support the liquid concrete, without the need of main formwork connected to the ground (Brozzetti, 2000). The main composite steel-concrete girders have elements that may suffer from local buckling (Ranzi & Zona, 2007), as in the case of steel plated double girders sections the web slenderness is around 120 (Davison & Owens, 2003). For box girders the situation is similar (Rya, Shimb, Change, & Chungc, 2004; Sherafati, Farimani, & Azizinamini, 2013), especially in the zone of negative bending moments in the compression flange (Ryu & Chang, 2005). To prevent these local effects many designers adopt the use of longitudinal stiffeners, creating smaller panels less prone to local buckling issues (Tedesco, Stallings, & Tow, 1995).

In the latest years, several studies concerning the feasibility of hybrid girders solution have been performed and adopted (Davison & Owens, 2003; Veljkovic & Johansson, 2004), demonstrating once more the importance of an advance study of composite steel-concrete sections (Hendawi & Frangopol, 1994). To better address these problems, a study was promoted concerning the behaviour of composite steel-concrete sections (shown in Figs. 1 and 2), considering several non-linear phenomena in an innovative manner, that isn't usually directly considered by bridge designers. This will permit to achieve a more realistic and economic final design (H.-J. Kim, Kim, & Park, 2013; Salvador, 2008) . Those phenomena are: the local buckling of steel web and flanges (Reis & Camotim, 2012), concrete time-dependent properties such as creep and shrinkage (Granata, Margiotta, & Arici, 2013; Kalkan & Lee, 2013), the physically non-linear stress-strain relations of concrete (Sharifi, 2012; Uddin, Jameel, Sobuz, Islam, & Hasan, 2013), and the construction sequence. Software was developed using object oriented programming, in order to analyse bridge deck sections, in which its key characteristics are: flexibility, precision and simplicity. Since the connection between the concrete and steel materials was outside of the scope of this study, a total shear connection is considered; future developments might include this aspect.
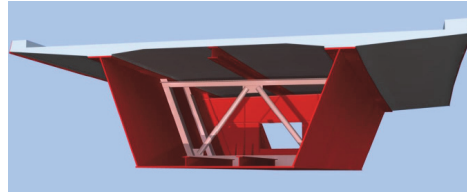

Fig. 1. Composite concrete-steel box girder

The section is divided using isolated elements. These elements come in various types of plates and materials which can be initially analysed separately, being later on grouped in order to achieve the global section behaviour. It is a similar approach to the domain division in the finite element method.

For this work only 7 type of elements where used, although since object oriented programing was used, it is very easy to add new elements, e.g.reinforced carbon fibers.
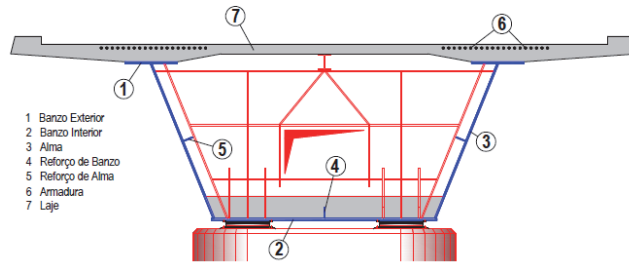

Fig. 2. Elements used in the analysis of the composite concrete-steel section

2. Constitutive Relations

Two types of materials were implemented, steel and concrete. For steel, a simple elastoplastic model with no hardening was used, with plastic strains. For concrete, the physically non-linear material behaviour was dealt in two parts: compression and tension. For compression a non-linear plasticity model proposed in Eurocode 2 was used for both serviceability and ultimate states. For the tension behaviour a simplified model of tension-stiffening was implemented for the serviceability states. Concrete creep and shrinkage was considered by adopting the curves proposed in Eurocode 2 (Ellingwood et al/, 2014).

2.1 Steel

The perfect elastoplastic behaviour stress-strain curve of the steel material is similar for both serviceability and ultimate state, the only difference residing in the yield stress value. Permanent plastic strains where considered and during unloading the stress-strain curve remains elastic with no hysteric loops.

$$\sigma_{sp}(\varepsilon_{sp}) = \begin{cases} -f_{spy} & \text{if} & -\varepsilon_{spu} < \varepsilon_{sp} < -\varepsilon_{spy} \\ E_{sp}\varepsilon_{sp} & \text{if} & -\varepsilon_{spy} \leq \varepsilon_{sp} \leq \varepsilon_{spy} \\ f_{spy} & \text{if} & \varepsilon_{spy} < \varepsilon_{sp} < \varepsilon_{spu} \end{cases} \tag{1}$$

The information regarding the mechanical properties, yield stress and strain are referred in Eurocode 3, these may depend on the thick of the plate being superior or inferior to 40mm. This limit is implemented in the software. Currently the range of grades of steel plate has increased with the introduction of high strength steels, exceeding 500 MPa yield strength, with new classes introduced namely S690, S960 and S1100.

For the reinforced steel rebars, a similar behaviour was implemented using the steel caraterisctis fixed in Eurocode 3. These are considered to be totally connected to the concrete, with no bond slip (Leonhardt, 1973; Montoya, Meseguer, & Cabré, 2002).

2.2 Concrete

2.2.1 Compression

In Eurocode 2 the stress-strain curve depends on the type of analysis being performed. For the ultimate state analysis, it is considered a non-linear plastic model without softening with a maximum ultimate strain (2), and the maximum compression stress is associated to its design value. Two strain limits are imposes, the first is associated to interval where hardening occurs, the second is associated to a perfect plasticity behaviour after the compression strain value is reached.

$$\sigma_c(\varepsilon_c) = \begin{cases} f_{cd}\left[1 - \left(1 - \dfrac{\varepsilon_c}{\varepsilon_{c2}}\right)^n\right] & \text{if} \quad 0 \le \varepsilon_c \le \varepsilon_{c2} \\ f_{cd} & \text{if} \quad \varepsilon_{c2} \le \varepsilon_c \le \varepsilon_{cu2} \end{cases} \tag{2}$$

For the serviceability state analysis a non-linear model is suggested in Eurocode 2 with a maximum compression stress associated to its average/characteristic value (3).

$$\sigma_c(\varepsilon_c) = f_{cm}\left(\frac{k\eta - \eta^2}{1 + (k-2)\eta}\right) \quad \text{if} \quad 0 \le \varepsilon_c \le \varepsilon_{cu1} \tag{3}$$

For both models the permanent strains aren't simulated, the hypothesis of linear unloading directly in the origin of the stress-strain curve is adopted. This hypothesis is adopted since Eurocode 2 provides no information concerning the unloading path.

2.2.2 Tension

For the tension behaviour a simple model of tension stiffening is adopted. This model assumes that concrete in tension still possesses some resistance after reaching tensile stress in reinforced concrete structures, more specifically in the resistance of concrete between cracks. Theses mechanisms of tension transmissions are difficult to assess, account and predict (Pina, 2009). The main issues on constitutive relations and modelling difficulties on the physical phenomena that governs the tension stiffening may be found in (Kwak & Filippou, 1990; Ratnamudigedara, 2002). In this work, a simple constitutive relation with no hardening and linear softening was implemented only for the serviceability limit state; for the ultimate limit no tension resistance is adopted. This model was based on the constitutive relation reported in the work of (Ratnamudigedara, 2002).

$$\sigma_c(\varepsilon_c) = \begin{cases} E_{cm}\varepsilon_c & \text{if} \quad 0 \le \varepsilon_c \le \varepsilon_{ctm} \\ f_{ctm} - \dfrac{f_{ctm}}{\varepsilon_{ctm}(\alpha - 1)}(\varepsilon_c - \varepsilon_{ctm}) & \text{if} \quad \varepsilon_{ctm} < \varepsilon_c \le \alpha\varepsilon_{ctm} \end{cases} \tag{4}$$

According to (Ratnamudigedara, 2002) several experimental results have shown that the α parameter varies between 6 and 28, in this work it was used $\alpha = 8$.

2.2.3 Shrinkage

As it is well known, some of concrete properties are time dependent. The mix of cement and water promotes the phenomena of shrinkage, in which the concrete tends to decrease its volume depending on the percentage of moisture in the air and the concrete size. In order to quantify the shrinkage the simplified model of Eurocode 2 is used in Eq. (5) that rely on decreasing strains.

$$\varepsilon_{cd}(t) = \beta_{ds}(t, t_s)k_h\varepsilon_{cd,0} + \varepsilon_{ca}(t) = \beta_{as}(t)\varepsilon_{ca,\infty} \qquad (5)$$

2.2.4 Creep

The creep effect occurs due to viscoelastoplasticity presented in the concrete, that may increase the strains is concrete due to compression stress along the time domain. This phenomenon is also simulated using the increasing of strain, presented in the simplified model in Eurocode 2 (6).

$$\varepsilon_{cc}(t, t_0) = \varphi(t, t_0)\frac{\sigma_c}{E_c} \qquad (6)$$

3. Plate Buckling

Next the EC3 methodology and the proposed method by the authors is presented and directly compared, namely using plate slenderness.

3.1 EC3 Methodology

The first concept of effective width was proposed by von Karman (von-Karman, Sechler, & Donnell, 1932), which admitted that the non-linear geometrical effect occurs in the longitudinal stress. The concept behind the effective width can then be described as the width of a fictitious plate subjected to a uniform stress distribution, which is statically equivalent to the nonlinear stress distribution in the actual plate installed, having the same value of maximum stress in both cases. In Eurocode 3, the elastic critical buckling stress in Eq. (7) depends on the plate support conditions and the stress distribution along the plate width, using the k parameter.

$$\sigma_{cr} = k\frac{\pi^2 E_{sp}}{12(1-v^2)}\left(\frac{t}{b}\right)^2. \qquad (7)$$

Since in Eurocode 3 the effective width is always computed for ultimate state limit, it is used the respective slenderness (8) formula concerning the plasticity of the plate. It is admitted that the effective area is keep constant through the loading history.

$$\bar{\lambda} = \sqrt{\frac{f_y}{\sigma_{cr}}} \qquad (8)$$

3.2 Proposed Method

In order to assess the flexibility of class 4 sections it is necessary to study the evolution of effective areas through the stress history. In service the effective areas are considerably larger than in ultimate state, but in Eurocode 3 this detail isn't covered which means that the computed displacements with class 4 sections are always upper values. The proposed method pretends to compute the evolution of the effective area along the stress history before it reaches the yield stress (Salvador, 2008). The methodology that was implemented calculates the slenderness of the plate depending on the stress level, or more specifically on the level of the maximum compression strain installed on the plate (9).

$$\bar{\lambda} = \sqrt{\frac{\varepsilon_{spc}E_{sp}}{\sigma_{cr}}} \qquad (9)$$

The use of the strain to compute the evolution of slenderness is adopted for the following reasons:

- The developed software was conceived in order to solve the non-linear systems using the strain field with the Bernoulli hypothesis.
- In the case of hybrid girders, the plates possess different yield stresses, therefore using the strain field it is possible to automatically take in to account this phenomenon during the iteration processes.
- Since in the Eurocode 3 methodology, the yield stress is used to compute level of slenderness in ultimate state limit, it seems reasonable to use the level of stress installed in the plate due to strain distribution considered in each iteration. In ultimate state limit analysis both methods provide the same result.

The reduction factor ρ follows the proposed formula in Eurocode 3. Two types of reduction factors are adopted: for internal compression plates (10); and for external compression plates (11).

$$\rho = \frac{\bar{\lambda} - 0,188}{\bar{\lambda}^2} \leq 1 \tag{10}$$

$$\rho = \frac{\bar{\lambda} - 0,055(3 + \psi)}{\bar{\lambda}^2} \leq 1 \tag{11}$$

The effective areas of compression plates are obtain using Table 4.1 and Table 4.2 of EC3-part 1.5 for internal and outstand members. The effective area of compression zone of a plate with the gross cross-sectional area A_c should be obtained from (12). The use of this methodology allowed once again obtaining the same results as the Eurocode 3 in ultimate state limits.

$$A_{c,eff} = \rho A_c \tag{12}$$

4. Algorithm Implementation

In order to implement the algorithm to solve the non-linear governing system at the section level, it is necessary to compute the axial and bending moment due to the strain distribution (Salvador, 2008). The integration of the stresses depends on the type of element being analysed. For flanges (steel and concrete) since the stresses are considered uniform along the thickness, it is easy to compute the axial stress (13) and bending moment (14). The value of y_i is referred to the gravity centre of the flange, and y is the coordinate of the point where the moment is computed.

$$N_i = b_{ef} t \sigma_{sp}(\varepsilon_i) \tag{13}$$

$$M_i = -b_{ef} t \sigma_{sp}(\varepsilon_i) \times (y_i - y) \tag{14}$$

For the steel web since the stresses varies along the height of the section, these must be integrated along the web area. For this work since a perfect elastoplastic model is used, it is possible to demonstrate that the axial stress and bending moment at the web are given by (15) and (16). The use of the angle α is due to the existence of tilted webs, mainly in box girders.

$$N_i = \left[(y_{sup} - y_{supplast}) \frac{\sigma_{sup} + \sigma_{supplast}}{2} + (y_{supplast} - y_{supint}) \frac{\sigma_{supplast} + \sigma_{supint}}{2} + (y_{infint} - y_{infplast}) \frac{\sigma_{infint} + \sigma_{infplast}}{2} \right.$$
$$\left. + (y_{infplast} - y_{inf}) \frac{\sigma_{infplast} + \sigma_{inf}}{2} \right] \frac{t}{\cos \alpha} \tag{15}$$

$$M_i = -\left[\left(\frac{y_{sup} + y_{supplast}}{2} - y \right) (y_{sup} - y_{supplast}) \frac{\sigma_{sup} + \sigma_{supplast}}{2} + \sigma_{supint} \frac{(y_{supplast} - y)^2 - (y_{supint} - y)^2}{2} \right.$$
$$+ \frac{\sigma_{supplast} - \sigma_{supint}}{y_{supplast} - y_{supint}} \left[\frac{(y_{supplast} - y)^3 - (y_{supint} - y)^3}{3} - (y_{supint} - y) \frac{(y_{supplast} - y)^2 - (y_{supint} - y)^2}{2} \right]$$
$$+ \sigma_{infplast} \frac{(y_{infint} - y)^2 - (y_{infplast} - y)^2}{2}$$
$$+ \frac{\sigma_{infint} - \sigma_{infplast}}{y_{infint} - y_{infplast}} \left[\frac{(y_{infint} - y)^3 - (y_{infplast} - y)^3}{3} - (y_{infplast} - y) \frac{(y_{infint} - y)^2 - (y_{infplast} - y)^2}{2} \right]$$
$$+ \left. \left(\frac{y_{infplast} + y_{inf}}{2} - y \right) (y_{infplast} - y_{inf}) \frac{\sigma_{infplast} + \sigma_{inf}}{2} \right] \frac{t}{\cos \alpha} \tag{16}$$

The web and flanges longitudinal stiffeners are only special cases of tilted webs and flanges, therefore its integration procedures are the same as (13), (14), (15) and (16). The procedures of the steel rebars are similar. For the steel web a simplified model adopted in Eurocode 3 is used to compute the axial stress and bending moment. All parameters of the web stress integration are presented in Fig. 3.
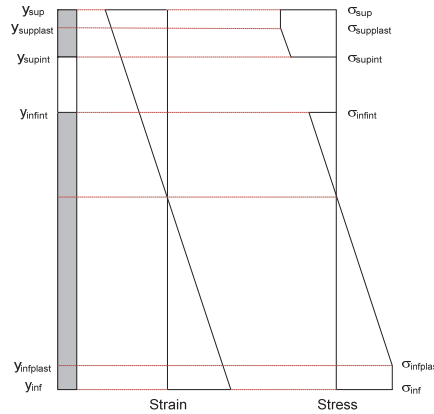

Fig. 3. Strain and stress variation along the high of a steel web.

After the integration of all stresses in all elements it is possible to compute the final values of axial force in Eq. (17) and bending moment in Eq. (18) acting in the section.

$$N = \sum N_{i\_web} + \sum N_{i\_flange} + \sum N_{i\_concrete} + \sum N_{i\_rebar} \tag{17}$$

$$M = \sum M_{i\_web} + \sum M_{i\_flange} + \sum M_{i\_concrete} + \sum M_{i\_rebar} \tag{18}$$

Several numerical algorithms where putted to the test, with the purpose of achieving convergence for any given load and providing a stable solution. After several attempts it was conclude that for this problem the combination between the three simple algorithms was the right choice in order to achieve convergence precision with low computational cost. The goal of these algorithms was to find a strain field that corresponds to a set of known internal forces (M, N) in non-linear analysis (Freitas, 1997). The main methodology of these algorithms is: imposing a initial random strain field; calculation the stress distribution in the section; verifying the computed error; new iteration through the adjustment of the strain field that depends on the upper ε_{sup} and lower strain ε_{inf} until the error is smaller than a given tolerance. These algorithms iterate around a fixed variable called pivot, whose value remains constant during a designated calculation step changing only the mobile variable. The first algorithm is called Double Pivot in which the roles can change passing from mobile variable to a pivot and vice-versa. In the Double Pivot algorithm, both values of the upper and lower strain are continued changed in the search of the correspondent set of known internal forces (M, N). The name of the algorithm comes from the fact that both variables may play the pivot role. Therefore this algorithm becomes more flexible because it allows the search of a strain field for 2 known variables (M, N). It is presented in Fig. 4 the flowchart for the iteration process; it is also displayed in Fig. 5 the evolution of the strain field with a given pivot during the iteration process.

The second algorithm is called Lower Pivot, in which the value of the lower strain is fixed, only modifying the value of the upper strain in the search of the strain field. Since only one variable is a pivot, only one boundary can be imposed in order to solve the constitutive problem at the section level, the other boundary must be fixed a priori. For this reason since in this work only beam sections are analysed, it is adopted as the 2nd boundary that the resulting axial stress is null $(N = 0)$. This algorithm is particularly useful when the section starts to yield; also it surpasses the difficulties of convergence of the Double Pivot when the variation of the strain field is much larger than the stress field. Some codes assign as ultimate limit state criteria a limitation of the maximum plastic strain of the upper/lower fiber, therefore this algorithm is ideal for these kinds of checks. It is presented in Fig. 6 a) the flowchart for the iteration process of the Lower Pivot; it is also displayed in Fig. 6 b) the evolution of the strain field with a given pivot during the iteration process.
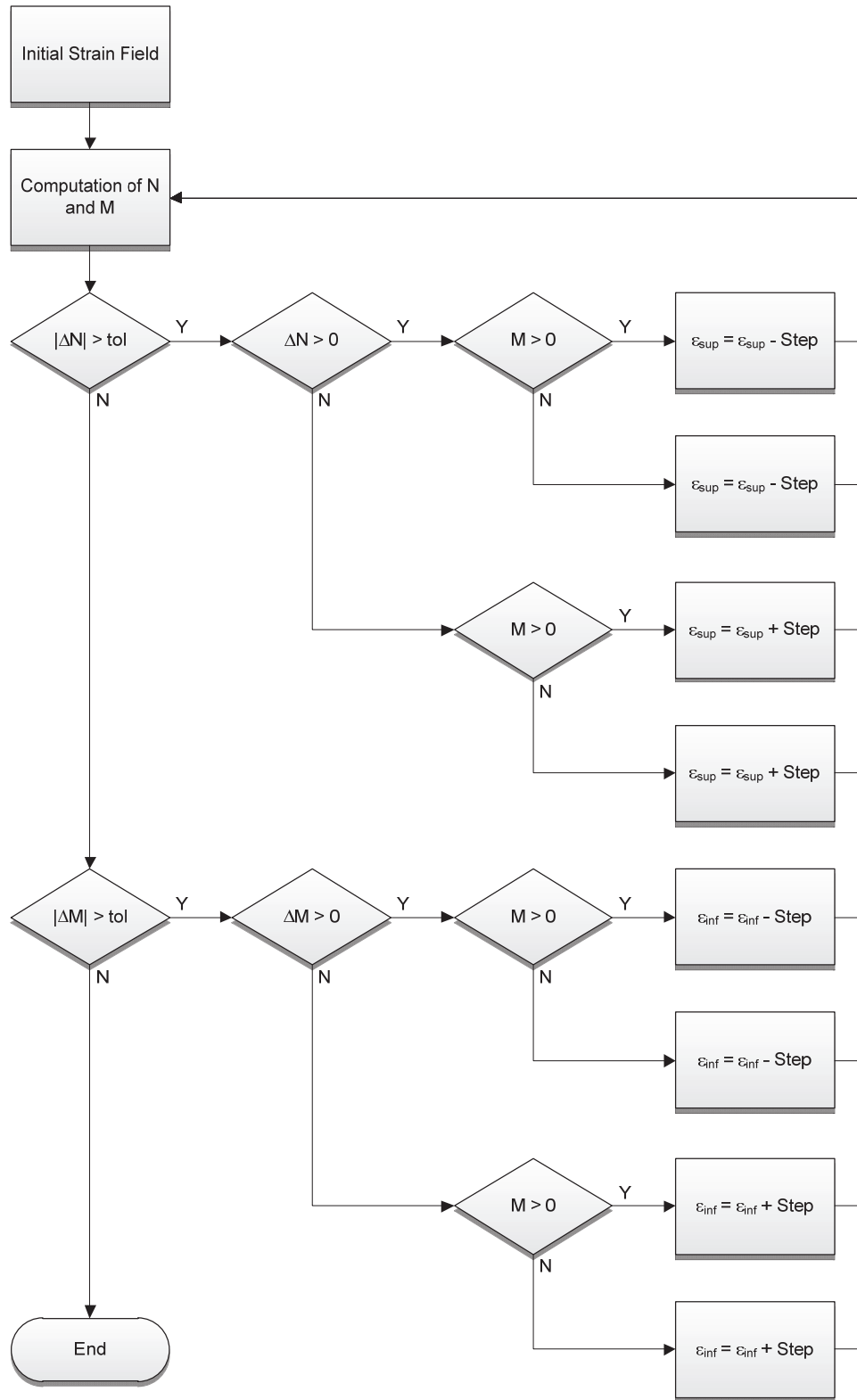
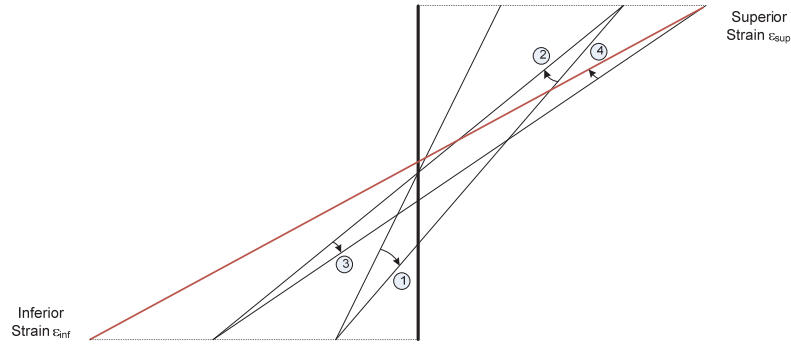**Fig. 4.** Flow chart of the double pivot algorithm

Fig. 5. Strain variation along the double pivot algorithm
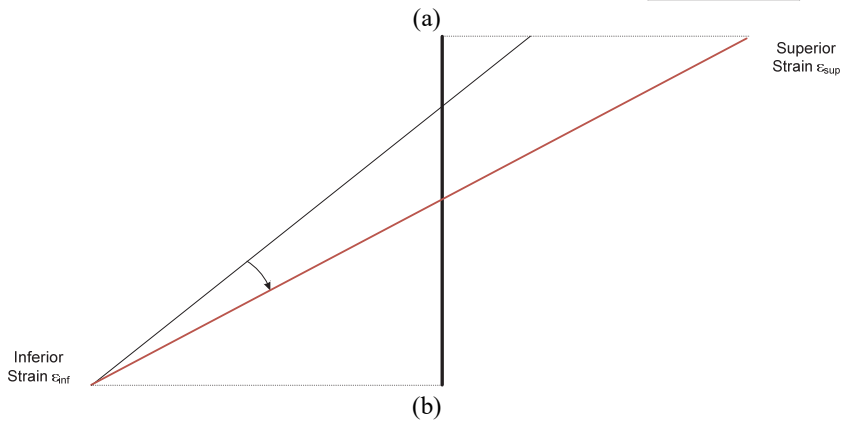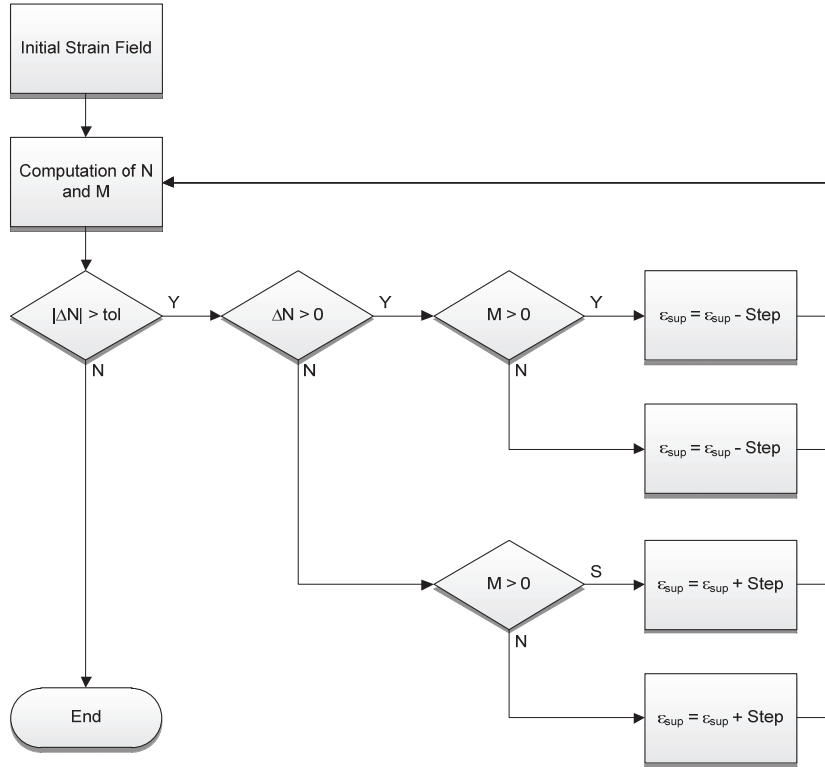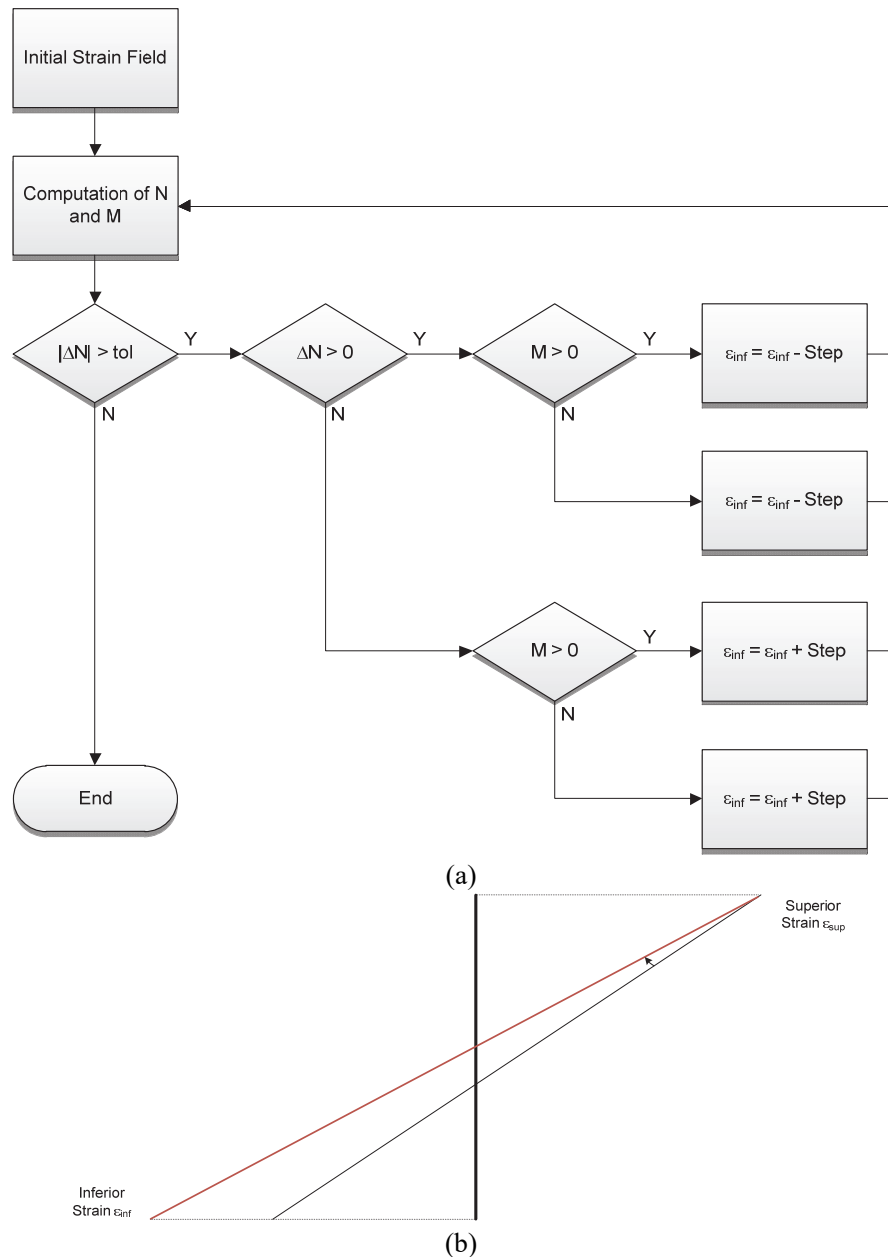

(a)

(b)

Fig. 6. a) Flow chart of the lower pivot algorithm b) Strain variation along the lower pivot algorithm

    The third algorithm is analogous to the previous one, and it is called Upper Pivot, in which the upper strain is fixed. It is presented in Fig. 7 a) the flowchart for the iteration process of the Upper Pivot; it is also displayed in Fig. 7 b) the evolution of the strain field with a given pivot during the iteration process.

Fig. 7. a) Flow chart of the lower pivot algorithm b) Strain variation along the lower pivot algorithm

5. Examples

Next four numerical examples are presented in order to validate the numerical model and present some contributions in the field of section analysis of composite steel-concrete structures. The first example concerns the comparison between the theoretical value of the resistance according to Eurocode 3, and the value computed with the proposed model. The second example is also a validation of a composite section, as presented in (Ministerio de Fomento, 2000). The third example studies the evolution of an effective area from the service state through the end of the ultimate limit state, in which an importance is given to achieve the real ultimate bending moment. The fourth example is a parametric application of the proposed method to composite box girder in order to study its serviceability limit state.

5.1 Model Validation HEB300

This example compares the bending moment-curvature relation for a rolled I-section subjected to bending moment in the y-y axis. It was used a standard HEB 300, which was calculated to the EC3 rules. Next an equivalent

section was introduced in the program and direct comparison was performed. The equivalent section did not consider the circular connection of the flange to the web.
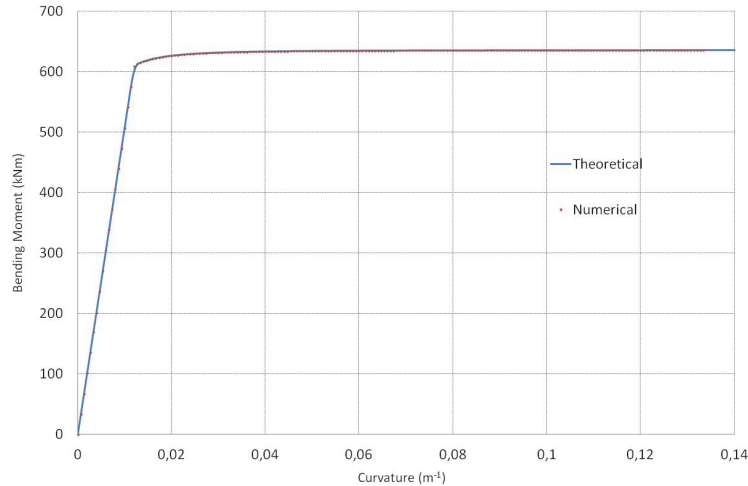

Fig. 8. Bending moment- curvature curve for the steel section

As seen in Fig. 8, the values obtain by numerical methodology are very similar to the ones obtain by analytical procedures of a simplified section, for both elastic and plastic zone. The main difference occurs near the first fiber to yield, this is due to the simplified area used in the numerical model. This difference is lower than +1.4% making it negligible for the global behaviour.

5.2 Model Validation with Composite Section

This example was presented in (Ministerio de Fomento, 2000). It concerns a composite steel-concrete section of plated girder with concrete flange at the top as presented in Fig. 9 a). The materials are S355 for the steel and C25/30 for the concrete. The construction phase is also simulated, in which at the beginning only provides stiffness and resistance.
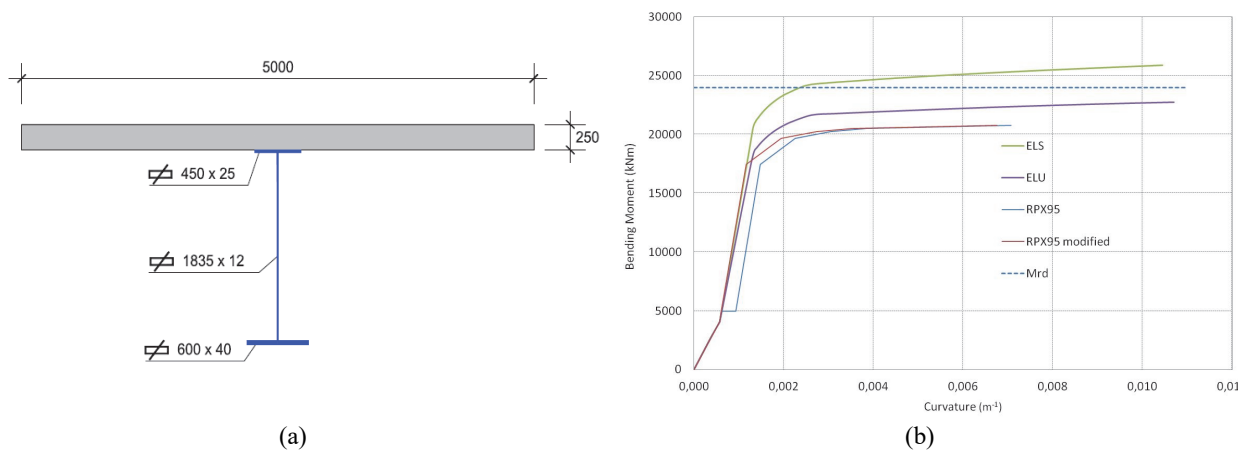

(a)   (b)

Fig. 9 – a) plated steel section, b) moment-curvature for various analysis cases

The performed analysis used the constitutive relations for both ultimate and serviceability limit states. A modified RPX curve was used because the original curve used creep and shrinkage functions that are different from the ones implemented in the algorithm. Observing Fig. 9 b) the serviceability limit state curve presented a good agreement with the RPX-modified curve. The key difference between the ultimate and serviceability limit state is concern with the different constitutive relations used. Although some differences still occur in the beginning of the yielding process when comparing the RPX curve and the numerical curve. The authors believe that this is due to: the use of homogenize section in the analytical model, which may not be correctly true due to the level of stress and strain in elastoplastic phase; the use of the same effective area for both ultimate and serviceability limit

state in the analytical calculation is not identical to the evolutive one computed with the proposed method. This produced and error lower to 7% in the elastoplastic phase.

5.3 Composite Concrete-Steel I Girder

The section in this test is similar to the previous one with different dimensions and the concrete slab possesses steel rebars that resist for both tension and compression (Fig. 10). It was adopted for plated steel S355 and for the concrete C40/50 with A500 for the steel rebars. Again the construction phase is also simulated, taking in to account the steel as formwork and the viscoelastoplasticity of creep and shrinkage. The values of relative moisture is 80%, the cement is type N, and the time analysis was performed for 50 years.
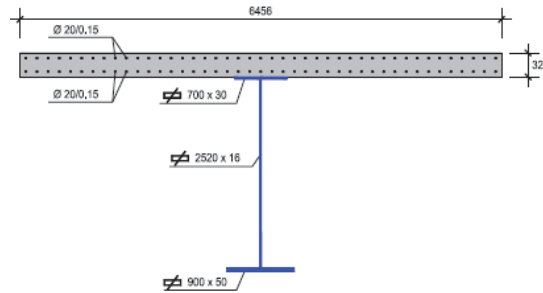

Fig. 10. Plated steel section in New Sado Bridge Crossing (approaching viaduct)

The performed analysis used the constitutive relations for the ultimate and serviceability limit states. Several graphics are plotted in order to study: the stress-strain curve; the evolution of the strain field; and the neutral axis along the yielding of the steel and concrete; the general influence of the class of concrete, the viscoelastoplasticity and the construction stage.

5.3.1 Positive bending moment study

With regard to the history load, the bending moment due to self weight is only supported by the steel plated section (Table 1). Only after the casting of the concrete, the slab and rebars start to contribute to the stiffness and the resistance of the section.

Table 1. Ultimate and service loads.

Bending Moments	Service Loads	Ultimate Loads
Dead Load	4260	5751
Extra Dead Load	5160	7740
Live Load	12270	18405

The first sets of six graphs are plotted for the serviceability limit state. In Fig. 11 a) it is easily distinguished the stiffness of the steel section alone, through its initial behaviour. Another clear known behaviour that can be also observed in Fig. 11 a), is the yielding of the composite section after de concrete cast, with an horizontal level. It is clear to conclude that from Fig. 11 b), that the first fiber to yield is the lower one, since the lower strain has a slope much steeper than the upper strain. On of the main consequences of different steep in the evolution of the upper and lower strain is the position of the neutral axis Fig. 11 c). When only the steel part of the section is activate the neutral axis position remains constant. Over time, neutral axis starts to shift because of the contribution of the slab and the rebars.

(a)   (b)   (c)
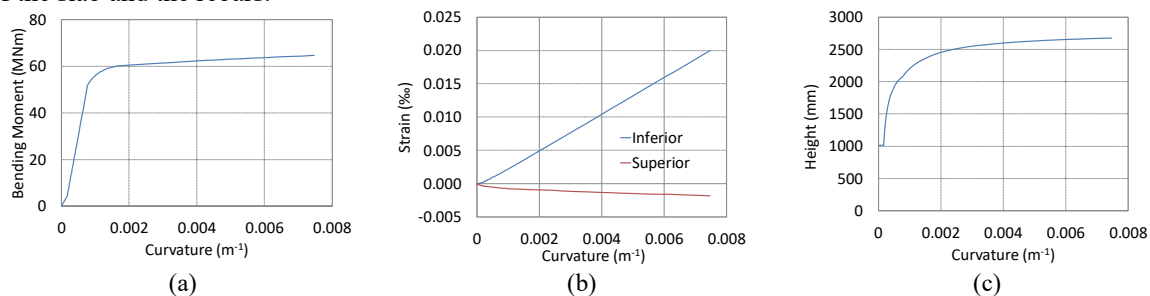
Fig. 11. Bending moment, curvature, flange strain and neutral axis position for service limit state

It is clearly displayed in Fig. 12 a) the evolution of the upper and lower stress in the steel plated section. Three main phases are distinguished: the first is the steel section working alone; in the second the stiffness of the full composite section starts responding; the third phase is the elastoplastic behaviour. The reason that the lower fiber in the slab is in tension Fig. 12 b), is due to the neutral axis being located at the slab after a given calculation step. Since this is an analysis using the serviceability limit state constitutive relationships, it is assumed that the tension stiffening occurs in concrete with softening; it is therefore admissible to observe in Fig. 12 b) that lower fiber in the slab has some resistance during tension behaviour. Another fact proves that the neutral axis is located in the concrete slab, is that the upper rebar is compressed but the lower rebar is tensioned. It is easy to conclude that the yielding process occurs in the inferior flange which presents and horizontal level, all the other control points regarding the superior flange, upper and lower concrete fibers and rebar present some nonlinearities, but none of them possess a horizontal stage.
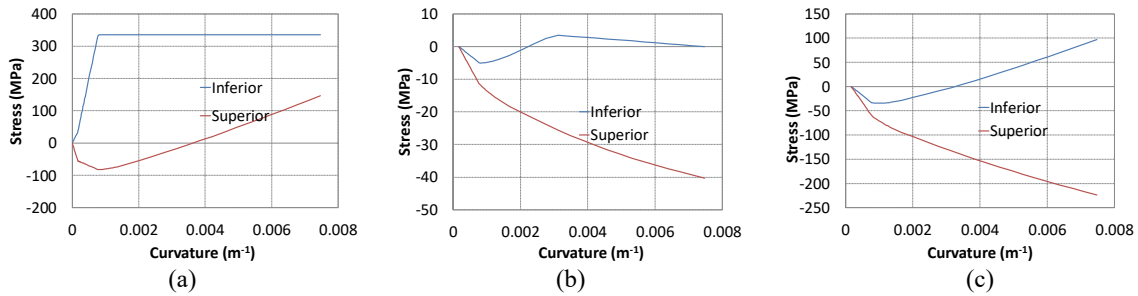

(a)   (b)   (c)

Fig. 12. Stresses in the steel, concrete flange and rebar for the service limit state

Next the same six graphs are plotted for the ultimate limit state Fig. 13. The conclusions are exactly the same, the biggest differences are the constitutive relationships of the concrete material. This is related in Fig. 14 b) where the lower concrete fibber doesnot possess any tension resistance; also the yielding process starts at the upper flange of the steel plated section Fig. 14 c). One of the main conclusions is that for very high plated girders it is almost impossible to reach the analytical M_{Rd} due to the fact that under the Bernoulli hypothesis the curvature must be $+\infty$, also it is recalled that under high strains this hypothesis is no longer valid. The numerical algorithm computed a value 8.7% lower than the analytical value for a maximum lower strain of 10‰, for a maximum lower strain of 20‰ the error of the numerical value computed is 5.3% lower than the analytical one.
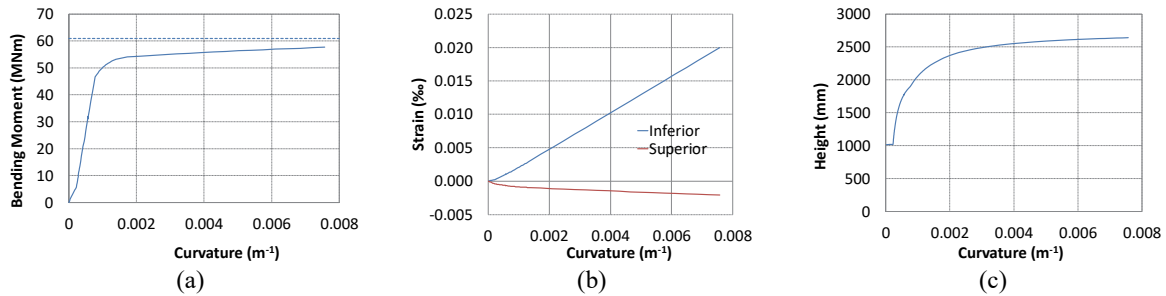

(a)   (b)   (c)

Fig. 13. Bending moment, curvature, flange strain and neutral axis position for ultimate limit state
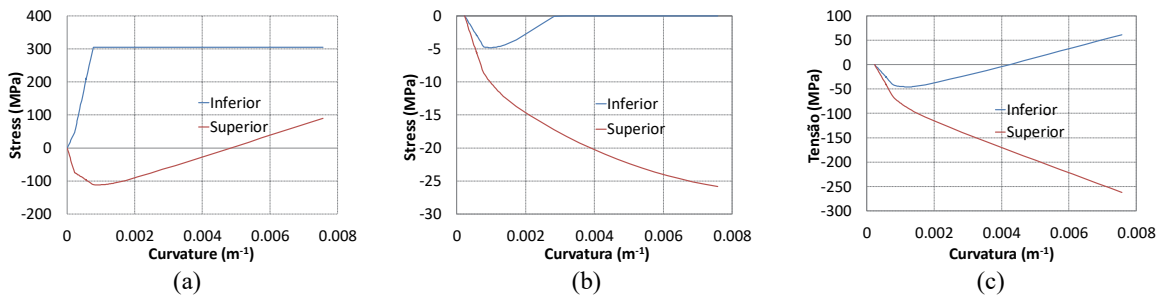

(a)   (b)   (c)

Fig. 14. Stresses in the steel, concrete flange and rebar for the ultimate limit state

Next a parametric study was performed in order to inquire the influence of the maximum compression resistance of the concrete, for the ultimate and serviceability limit state Fig. 15 a), Fig. 15 b). As stated before

although some nonlinearities may occur in the concrete fibers, its influence for the M_{Rd} are minor since the steel yields first. Another parametric study was executed concerning the % of self weight applied in the construction stage Fig. 15 c), Fig. 16 a). The composite stiffness occurs at different time steps, but its value is identical for all three cases, also the value of M_{Rd} for 300% is lower than 100% but very similar.
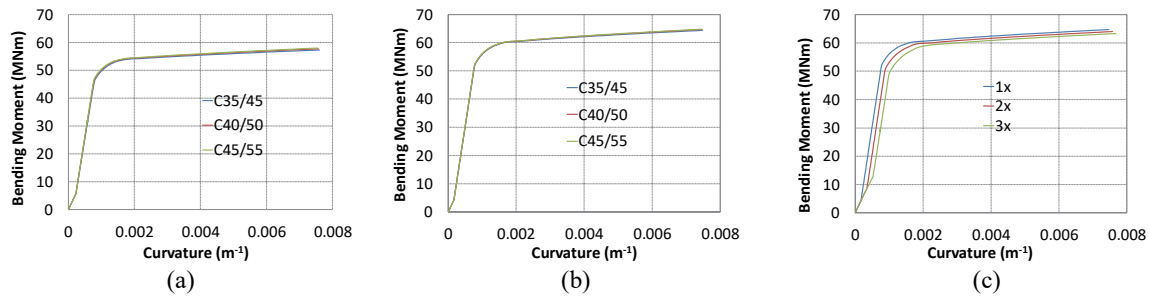

Fig. 15. Bending Moment for different class of concrete in ultimate a) and service limit state b), and influence of the construction stage for the service limit state c)

The effects of viscoelastoplasticity were also inquired in order to study its effects for serviceability and ultimate limit states. It was considered a model with and without viscoelastoplasticity Fig. 16 b), Fig. 16 c). The value of M_{Rd} is identical for both variation, minor differences appears in the elastic zone.
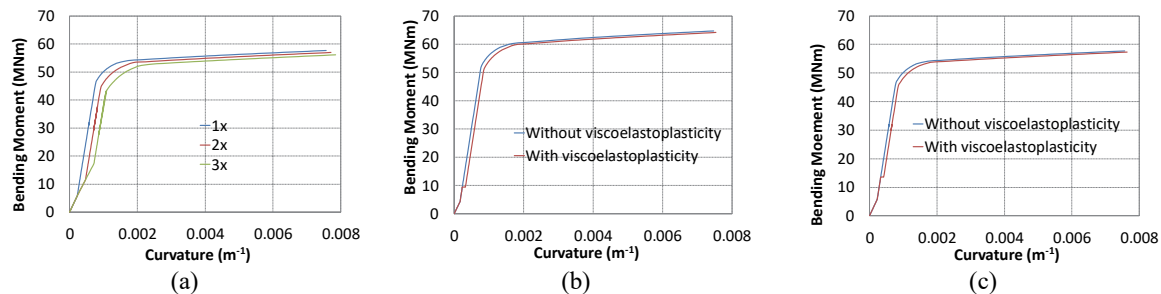

Fig. 16. Influence of the construction stage for the ultimate limit state a) and effects of the viscoelastoplasticity for the service and ultimate limit state

5.3.2 Negative bending moment study

For the negative bending moments some problems of convergence with conventional Newton-Raphson algorithms may occur for the moment-curvature curve, since softening occurs. This kind of behaviour is ideal to be treated with a combination of Double Pivot with Fixed Pivot.

Table 2. Ultimate and service loads

Bending Moments	Service Loads	Ultimate Loads
Dead Load	-9220	-12447
Extra Dead Load	-11670	-17505
Live Load	-14610	-21915

The first sets of six graphs are plotted for the serviceability limit state. Once again the construction stage where the steel section is used as formwork is clearly visible Fig. 17 a). The composite section suffers a decrease of stiffness around 30000 kNm, this happens because the maximum tension load of the concrete f_{ctm} is reached. A clear softening is present for a maximum bending moment of 63000kNm this behaviour happens because that the effective area tends to decrease with the motion of the neutral axis with the yielding of the lower flange Fig. 17 c). After this step an increase of strain produces a decrease of bending moment, since the upper strains increases slower than the lower strain Fig. 17 b). Just like in the previous case the position of the neutral axis remains constant during the construction phase. When the concrete is cast and the composite section starts working the neutral axis rises until the maximum tension of the concrete is achieved, after that it descends moving to the position of the neutral axis considering only the existence of steel rebar in the slab and the steel section. Later when the lower flange begins to yield the neutral axis rises once again.
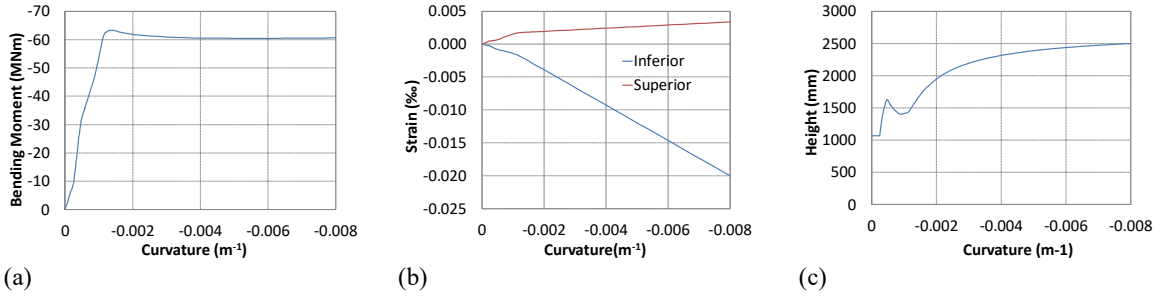
Fig. 17. Bending moment, curvature, flange strain and neutral axis position for service limit state

The tension in the upper flange decreases when the lower flange yields Fig. 18 a). As the effective area decreases with the increase in the level of strain in the section, it is then expected a softening branch in the bending moment-curvature Fig. 18 b). Therefore, in order to recover equilibrium at the section level the neutral axis must rise, diminishing the resulting bending moment.
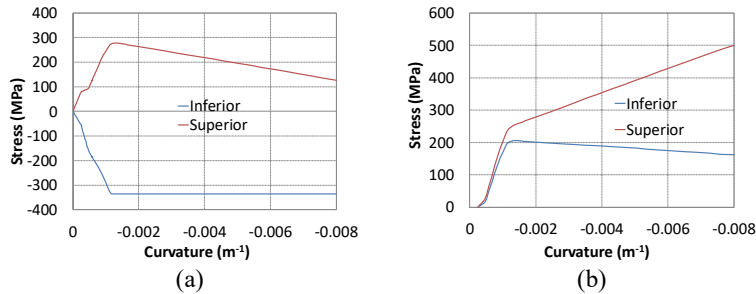

Fig. 18. Stresses in the steel and rebar for the service limit state

For the ultimate limit state the conclusions and behaviours are identical Fig. 19 a), Fig. 19 b). The main difference occurs in the evolution of the position of the neutral axis, since for ultimate limit state the concrete doesnot possess any resistance in tension, its variation is much smother Fig. 19 c). Again just like in the positive bending moment it was not possible to reach the analytical negative M_{Rd} Fig. 19 a). Fig. 20 also shows the stress profile for the steel and rebar ultimate limit state.
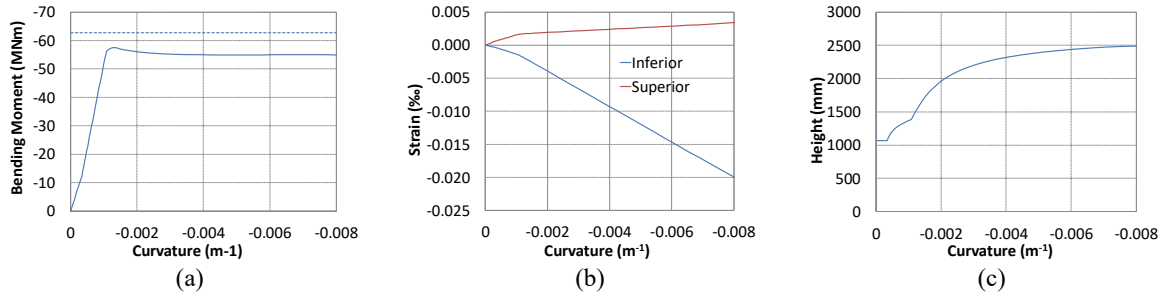

Fig. 19. Bending moment, curvature, flange strain and neutral axis position for ultimate limit state
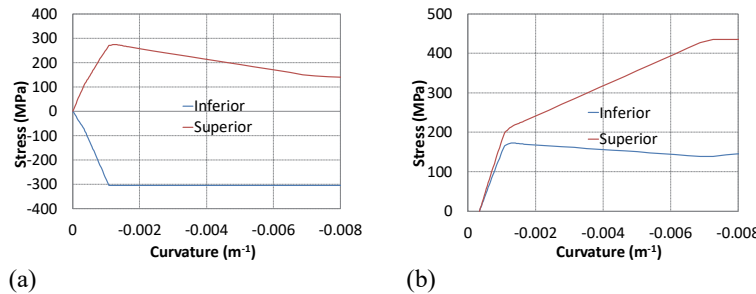

Fig. 20. Stresses in the steel and rebar for the ultimate limit state

5.4 Composite Concrete-Steel Box Girder

Next the proposed methodology is tested with a composite steel-concrete box girder. For this example only the serviceability limit state is evaluate (see Fig. 21). This box girder was used in a study for bridge in Belgium, therefore its design load values are represented in Table 3.
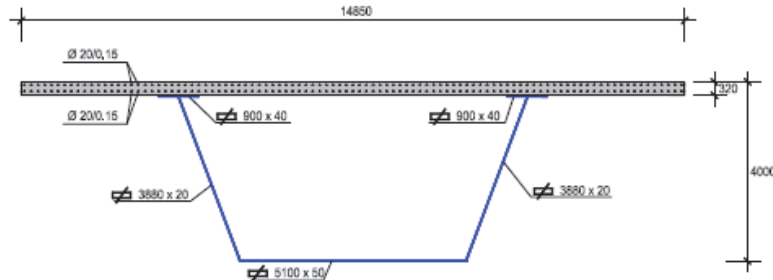

Fig. 21. Composite concrete-steel box girder

Table 3. Ultimate and service loads

Bending Moments [kNm]	Service Load
Dead Load	96310
Extra Dead Load	33220
Live Load	56610

For this section the dead weight load is particular high before the concrete is cast. This can be observed in Fig. 23 a) in which for the construction stage the maximum compression of the upper flange is around 300 MPa. After the cast the concrete flange, it starts to contribute to the stiffness and resistance of the section, and the compression of the upper flange is reduced. It is also displayed in Fig. 22 c) the evolution of the neutral axis, in which during the construction stage it descends due to a decrease in the effective area of the steel section. After the cast the neutral axis rises and the effective area increases dramatically, and converges to a stable value. The consequences of the heavy dead load in the construction stage may be observed in Fig. 22 b), in which a quick evolution of the upper strain is noted, which may lead to a increase of vertical displacement of the structure. This is a rare example that shows the importance of correctly analysing the evolution the dead weight during the construction stage and its impact on future strains and displacements. It is therefore important to suggest in Eurocode 4 a maximum limit of the steel stress during the construction stage.
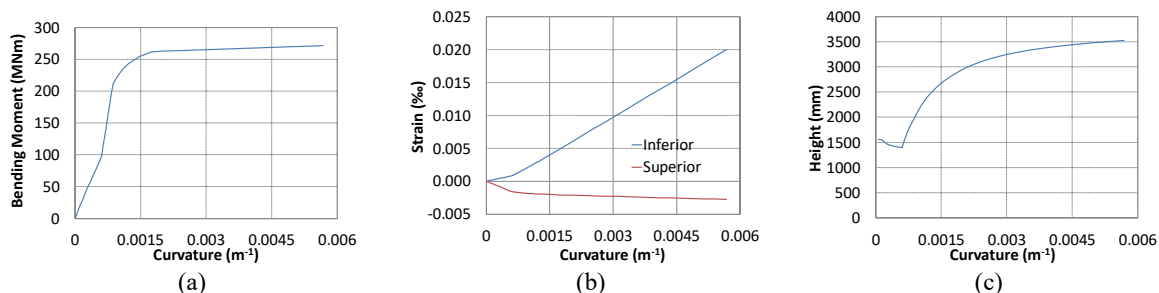

(a)   (b)   (c)

Fig. 22. Bending moment, curvature, flange strain and neutral axis position for service limit state
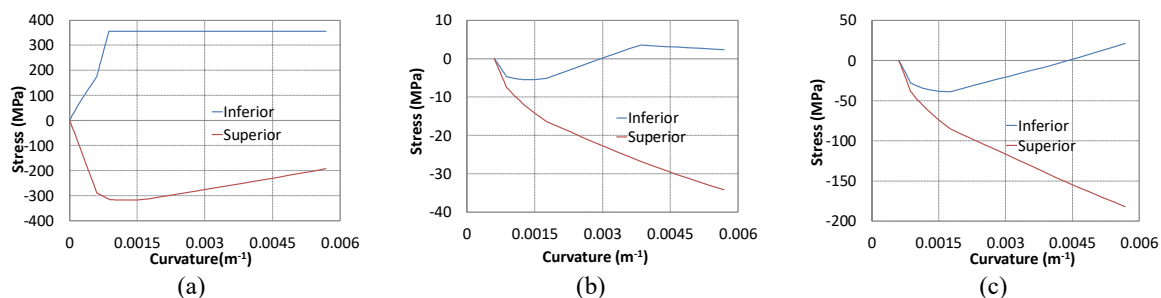

(a)   (b)   (c)

Fig. 23. Stresses in the steel, concrete flange and rebar for the service limit state

6. Conclusions and Further Developments

For this work it was developed software that allows a new approach to solve the computation of class 4 section composite steel-concrete sections. This approach consisted in the computation of the evolutive behaviour of a composite section, taking to account its loading history, through the incremental analysis of strains using the Bernoulli hypothesis. This new approach involved the adaptation of existing regulations in order to create a coherent whole. The proposed method was validated using several examples. The proposed methodology demonstrated that the use of the entire plastic section tends to overestimate. This is due to the fact that for the entire theoretical plastic section admits that the value of the strain and curvature of the extreme fibbers tends to infinite. This overestimation tends to grow with the height of the section; therefore, it is proposed an artificial reduction coefficient for the calculation of M_{Rd} for higher sections. The construction stage presents some importance in the final behaviour of the composite section namely in the decrease of the ultimate resistant bending moment. This reduction increases if the concrete slab interaction with the steel section tends to start later. Also it was observed that is the stress level in steel during the construction stage are high, these present some consequences in the evolutive behaviour of class 4 sections, which can be translated to excessive deformations and the appearing of local instabilities during the beginning of its useful life. The level of the effective area is clearly higher for the serviceability state limit, therefore the flexibility of the section for the analysis of displacements tends to diminish when compared with the effective are in ultimate state limit.The success and innovation observed during the results presented in this work have pushed this researched team to developed further studies on this theme of structural engineering. Future developments of this work are already in course namely: interaction with shear stress, which may have some importance in the decreasing of resistant bending moment and increasing of effective area in class 4 sections; using numerical and experimental results to calibrate a new parameter k for the elastic buckling stress, especially in internal web which are partially fixed in the flanges and webs partially fixed in concrete slabs; the extension to the frame element in order to compute with more accuracy the displacements and plastic hinges of class 4 girders, including plasticity and local instabilities; the study of the proposed methodology in hybrid girders in order to directly inquirer its benefits; the evolution of class 4 sections for cycle loads in the presence of axial and bending stresses.

Acknowledgements

References

Anitori, G., Casas, J., & Ghosn, M. (2013). Redundancy and Robustness in the Design and Evaluation of Bridges: European and North American Perspectives. *Journal of Bridge Engineering, 18*(12), 1241-1251. doi: doi:10.1061/(ASCE)BE.1943-5592.0000545

Bradford, M.A., Uy, B., & Pi, Y. (2001). Behaviour of unpropped composite girders curved in plan under construction loading. *Engineering Structures, 23*(7), 779-789. doi: 10.1016/S0141-0296(00)00097-3

Brozzetti, J. (2000). Design development of steel-concrete composite bridges in France. *Journal of Constructional Steel Research, 55*(1-3), 229-243. doi: 10.1002/stab.199903170

Davison, B., & Owens, G.W. (2003). *Steel Designers' Manual*, (6th ed.): Backwell science.

Ellingwood, B., Vrouwenvelder, T., & Gulvanessian, H. (2014). Eurocodes and their implications for bridge design: Background, implementation, and comparison to North American practice. *Journal of Bridge Engineering, 19*(1), 3-4. doi: doi:10.1061/(ASCE)BE.1943-5592.0000567

Freitas, J.A.T. (1997). *Calculo Automático de Estruturas*. Lisboa: Instituto Superior Técnico.

Granata, M., Margiotta, P., & Arici, M. (2013). Simplified procedure for evaluating the effects of creep and shrinkage on prestressed concrete girder bridges and the application of European and North American prediction models. *Journal of Bridge Engineering, 18*(12), 1281-1297. doi: doi:10.1061/(ASCE)BE.1943-5592.0000483

Hendawi, S. , & Frangopol, D.M. (1994). Design of composite hybrid plate girder bridges based on reliability and optimization. *Structural Safety, 15*(1-2), 149-165. doi: 10.1016/0167-4730(94)90057-4

Kalkan, Ilker, & Lee, Jong-Han. (2013). Effect of shrinkage restraint on deflections of reinforced self-compacting concrete beams. *KSCE Journal of Civil Engineering, 17*(7), 1672-1681. doi: 10.1007/s12205-013-1007-4

Kim, Hyun-Joong, Kim, Ho-Kyung, & Park, JunYong. (2013). Reliability-based evaluation of load carrying capacity for a composite box girder bridge. *KSCE Journal of Civil Engineering, 17*(3), 575-583. doi: 10.1007/s12205-013-0603-7

Kim, K., & Yoo, C.H. (2006). Effects of external bracing on horizontally curved box girder bridges during construction. *Engineering Structures, 28*(12), 1650-1657. doi: 10.1016/j.engstruct.2006.03.001

Kwak, H.G., & Filippou, F.C. (1990). *Finite Element Analysis of Reinforced Concrete Structures under Monotonic Loads* (Vol. Report no. UCB/SEMM-90/14). University of California (Berkeley).

Leonhardt, M. (1973). Construcções em concreto armado (Vol. 1,2,3,4,5 and 6). Rio de Janeiro: Editora Interciencia LTDA.

Ministerio de Fomento. (2000). Manual de applicación de lasRecomendaciones RPM – RPX / 95. Ministerio de Fomento, Secretaria de Estado de Infraestructuras y Transportes: Dirección General de Carreteras, Anejo nº1, páginas 1.1 a 1.23.

Montoya, P.J., Meseguer, A.G., & Cabré, F.M. (2002). Hormigón Armado: Editora Gustavo Gili.

Pedro, J.J.O., & Reis, A.J. (2010). Nonlinear analysis of composite steel–concrete cable-stayed bridges. *Engineering Structures, 32*(9), 2702-2716. doi: 10.1016/j.engstruct.2010.04.041

Pina, J.P.P. (2009). Structural Assessment of Corroded RC Structures Through Numerical Modelling. (Ph.D Thesis), Instituto Superior Técnico, Lisboa.

Ranzi, G., & Zona, A. (2007). A steel–concrete composite beam model with partial interaction including the shear deformability of the steel component. *Engineering Structures, 29*(11), 3026-3041. doi: 10.1016/j.engstruct.2007.02.007

Ratnamudigedara, P. (2002). *Crack spacing, crack width and tension stiffening effect in reinforced concrete beams and one-way slabs*. (Ph.D. Thesis), Griffith University.

Reis, A.J. (1997). Pontes Metálicas e Mistas: Desenvolvimentos e Realizações. Paper presented at the Encontro Nacional de Construção Metálicas e Mista, Porto Portugal.

Reis, A.J. (1999). Pontes Mistas Aço-Betão. Paper presented at the Encontro Nacional de Construção Metálica e Mista, Coimbra Portugal.

Reis, A.J. (2005). Pontes Mistas: Desenvolvimentos e Projectos Recentes. Paper presented at the Congresso de Construção Metálicas e Mista, Lisboa Portugal.

Reis, A.J., & Camotim, D. (2012). Estabilidade e Dimensionamento de Estruturas. Lisboa: Orion.

Reis, A.J., & Pedro, J.J.O. (2004). The Europe Bridge in Portugal: concept and structural design. *Journal of Constructional Steel Research, 60*(3-5), 363-372. doi: 10.1016/S0143-974X(03)00116-0

Rya, H.K., Shimb, C.S., Change, S.P., & Chungc, C.H. (2004). Inelastic behaviour of externally prestressed continuous composite box-girder bridge with prefabricated slabs. *Journal of Constructional Steel Research, 60*(7), 989-1005. doi: 10.1016/j.jcsr.2003.09.004

Ryu, H.K., & Chang, S.P. (2005). Ultimate strength of continuous composite box-girder bridges with precast decks. *Journal of Constructional Steel Research, 61*(3), 329-343. doi: 10.1016/j.jcsr.2004.08.003

Salvador, L. (2008). Análise e Comportamento Evolutivo de Secções Mistas Aço-Betão em Tabuleiros de Pontes. (M.Sc.), Instituto Superior Técnico, Lisbon.

Sharifi, Y. (2012). Structural performance of Self-Consolidating Concrete used in reinforced concrete beams. *KSCE Journal of Civil Engineering, 16*(4), 618-626. doi: 10.1007/s12205-012-1517-5

Sherafati, A., Farimani, R., & Azizinamini, A. (2013). Effect of concrete slab on shear capacity of composite plate girders under positive moment. *Journal of Bridge Engineering, 18*(2), 89-98. doi: doi:10.1061/(ASCE)BE.1943-5592.0000319

Tedesco, J.W., Stallings, J.M., & Tow, D.R. (1995). Finite element method analysis of bridge girder-diaphragm interaction. *Computer & Structures, 56*(2-3), 461-473. doi: 10.1016/0045-7949(95)00037-H

Uddin, Md Alhaz, Jameel, Mohammed, Sobuz, HabiburRahman, Islam, Md Shahinul, & Hasan, NoorMd Sadiqul. (2013). Experimental study on strength gaining characteristics of concrete using Portland Composite Cement. *KSCE Journal of Civil Engineering, 17*(4), 789-796. doi: 10.1007/s12205-013-0236-x

Veljkovic, M., & Johansson, B. (2004). Design of hybrid steel girders. *Journal of Constructional Steel Research, 60*(3-5). doi: 10.1016/S0143-974X(03)00128-7

von-Karman, T., Sechler, E.E., & Donnell, L.H. (1932). The Strength of Thin Plates in Compression. Transactions of the American Society of Mechanical Engineers (ASME), 54, 53.